DesAgent: A Multi-Agent Mechanical Design Method Based on Collaborative Large and Small Models

Lead Author: Shijie Zhang

School of Mechanical Engineering, Tiangong university, Tianjin, 300387, China.

Email: zsj1491066330@outlook.com

Corresponding Author and Co-Author: Xinrong Li

School of Mechanical Engineering, Tiangong university, Tianjin, 300387, China.

Email: lixinrong@tiangong.edu.cn

Co-Author: Chengxu Yuan

School of Mechanical Engineering, Tiangong university, Tianjin, 300387, China.

Email: YuanCx999@hotmail.com

Co-Author: Wenqian Feng

School of Mechanical Engineering, Tiangong university, Tianjin, 300387, China.

Email: fengqian2204@163.com

Co-Author: Quansheng Jiang

School of Mechanical Engineering, Tiangong university, Tianjin, 300387, China.

Email: 1711819201@qq.com

ABSTRACT

Mechanical design today faces critical challenges in design efficiency and multidisciplinary optimization, often constrained by high computational costs and fragmented processes. To address these issues, this paper proposes DesAgent, a multi-agent collaborative design methodology that integrates the semantic reasoning capabilities of Large Language Models (LLMs) with the numerical prediction accuracy of Reduced-Order

Small Models (ROSMs). The proposed approach constructs a Semantic-Numerical Synergy Loop (SNS-Loop), enabling a closed-loop, intelligent design process that bridges semantic interpretation and numerical validation. DesAgent features a hierarchical multi-agent system consisting of four specialized agents—Requirements Analyst, Task Planner, Designer, and Feedback Evaluator—each responsible for a distinct phase of the design pipeline. The LLMs support natural language parsing and task planning, while the ROSMs ensure real-time simulation-level predictions through neural network-based surrogate models. To validate the proposed methodology, a case study on the structural optimization of a spinning frame wall plate is conducted. Experimental results show that DesAgent reduced material consumption by 21.2% while satisfying multiple constraints related to stress, deformation, and natural frequency avoidance. The entire design optimization process completed in 232 seconds, consuming only 12,044 tokens of computational resources. This work presents an efficient, low-cost, and generalizable design framework that demonstrates the feasibility of LLM-augmented collaborative intelligence in complex mechanical design tasks.

Keywords: *large language models (LLMs); reduced-order small models (ROSMs); multi-agent systems; collaborative mechanical design; structural optimization*

1 Introduction

Mechanical design serves as a fundamental pillar of modern manufacturing, playing a critical role in the iterative development of complex mechanical systems [1]. Traditionally, the design process has relied heavily on the expertise and reasoning skills of human designers, often resulting in prolonged design cycles and increased development costs [2]. Existing approaches—such as experimental methods, simulation-driven design, and AI-assisted techniques—face notable limitations. Experimental methods incur high trial-and-error costs due to the need for physical prototypes [3,4]. Simulation-based design approaches, although widely used, suffer from discrepancies between idealized simulation environments and real-world operating conditions [5,6], making it difficult to achieve accurate and efficient multidisciplinary coordination. Surrogate model–based methods [7,8], while computationally efficient, often fail to capture the highly nonlinear relationships among a large number of design variables and performance responses.

To overcome these challenges, the development of efficient, collaborative, and intelligent design frameworks has become increasingly vital. Recent advances in Large Language Models (LLMs) have enabled new paradigms for intelligent design by leveraging their powerful semantic understanding and task

planning capabilities. One widely adopted approach involves role-based multi-agent collaboration, where multiple specialized agents decompose and execute tasks sequentially [9,10]. However, such paradigms often lack the ability to perform accurate numerical calculations, limiting their effectiveness in engineering design tasks. Another research stream attempts to enhance LLMs with function libraries [11,12]. However, analytic formulas alone are insufficient to reflect complex structural responses—such as stress distribution, displacement fields, and modal characteristics—that usually require numerical simulations. LLMs combined with professional simulation software [13,14] can capture these responses, but the computation time grows rapidly with structural complexity, thereby lowering design efficiency. In addition, LLM-driven frameworks that leverage external surrogate models [15,16] are often unidirectional: surrogate models are used only to validate completed designs, lacking the iterative refinement required in optimization-intensive engineering tasks.

To address these limitations, this study introduces DesAgent, a novel multi-agent mechanical design method. It should be noted that conventional LLM-based API calling approaches face inherent weaknesses in iterative optimization, since they typically operate on single-turn calls without continuous feedback control. Moreover, LLMs are not inherently capable of accurate numerical prediction (e.g., stress, deformation, modal frequencies), which makes them insufficient for quantitative verification in mechanical design. Finally, when multiple tasks such as material selection, structural analysis, and modal analysis are interdependent, traditional single-agent frameworks struggle to resolve coupling and coordination. These challenges highlight the necessity of introducing a collaborative multi-agent architecture, even for relatively simple parametric optimization problems. Therefore, this study evaluates DesAgent as an autonomous design workflow that pairs surrogate-enabled fast numerical loops with LLM-driven requirement parsing, conflict resolution, and task scheduling to maintain feasibility under multi-constraint, multidisciplinary coupling.

2 DesAgent: Collaborative Large and Small Model Design Method

This chapter serves as the core of the methodology and details the implementation mechanisms and technical pathways of DesAgent. Centered on the dual-loop collaborative architecture of the Semantic–Numerical Synergy Loop (SNS-Loop), the framework integrates two complementary cycles: (i) a semantic reasoning loop, where LLM-based agents interpret requirements, decompose tasks, and generate candidate design strategies; and (ii) a numerical validation loop, where ROSM-based agents provide rapid simulation-

level predictions and constraint checking. These two loops operate in close interaction, with semantic reasoning guiding exploration and numerical feedback supporting refinement, thereby forming a collaborative and iterative optimization process. Accordingly, this chapter provides an in-depth analysis of three core components: (1) the LLM-driven automated design paradigm, (2) the hierarchical multi-agent collaboration mechanism, and (3) the ROSM-based modeling method.

2.1 DesAgent Architecture

The architecture of DesAgent, illustrated in Fig. 1, is organized into four functional modules: Zone A (User Input Area) receives user-defined design requirements and constraints, including initial parameters, performance objectives, and boundary conditions; Zone B (Task Analysis Area) employs the Requirements Analyst agent to interpret engineering semantics from user inputs through a multidisciplinary coupling analysis. This process generates structured and executable design tasks; Zone C (Subtask Execution Area) utilizes the Task Planner agent to construct a task flow based on parameter dependencies and coupling relationships. The planner decomposes the global design objective into discipline-specific subtasks, which are executed by specialized agents (e.g., structural designer, process optimizer) through the dynamic invocation of tools such as ROSMs, iterative validators, and component libraries; Zone D (Output Area) compiles and delivers the final outputs, including the optimized design solution, process logs, and multidimensional validation reports (e.g., mechanical performance, manufacturability). To ensure robust and efficient iteration, a multi-agent feedback coordination mechanism operates across Zones B and C, dynamically verifying intermediate outputs and enabling real-time correction within the SNS-Loop.

To quantify the information flow in the user input area (Zone a), a state-space model for the user input layer is defined:

$$S_a = (Q, C) \tag{1}$$

In this equation, the semantic feature vector Q=A_{PT}(*user-input*) is extracted by Agent A_{PT} using prompt techniques to capture user semantic requirements (e.g., lightweight and high strength). It is mapped to $Q \in R^m$, where m represents the feature dimension. The constraint structured encoding C=(C_{state},C_{value}), where $C_{state} \in \{0,1\}^k$ indicates whether each constraint is active (C_{state}=1 means the constraint is enabled and must be enforced in the current design task, while C_{state}=0 means it is inactive and temporarily ignored), and $C_{value} \in R^k$ stores the corresponding constraint thresholds or category encodings (k is the total number of constraints).

Based on the output S_a from the user input layer, the Task Analysis Area (Area b) resolves conflicts arising from multidisciplinary requirements (e.g., the conflict between lightweight mechanical goals and process feasibility constraints). By defining a multidisciplinary coupling matrix $\boldsymbol{W}_G$, conflicting requirements from the user end are mapped to conflict-free subtasks for the agents. The state S_b of the task analysis layer and the user input S_a satisfy the following equation:

$$S_b = \boldsymbol{W}_G \cdot S_a \tag{2}$$

Key technical details and symbol explanations are as follows: The multidisciplinary coupling matrix $\boldsymbol{W}_G \in R^{n\times(m+q)}$, where n is the number of disciplines (e.g., mechanics, materials, processes), m is the dimension of design variables (e.g., geometric parameters), and q is the dimension of constraints. The matrix is dynamically updated using a Retrieval-Augmented Generation (RAG) knowledge base. The iterative update rule is:

$$\mathbf{W}_G^{t+1} = \mathbf{W}_G^{t} + \eta \cdot \mathrm{RAG}(\epsilon_s) \tag{3}$$

Here $\eta=\partial L_{RAG}/\partial t=[L_{RAG}(t)-L_{RAG}(t\text{-}1)]/\Delta t$ represents the knowledge update rate, and the semantic deviation ϵ_s is defined as the Frobenius norm of the difference between the discipline demand matrices of adjacent iterations: $\epsilon_s=\|M^{(t)}-M^{(t\text{-}1)}\|_F$, where $M^{(t)}$ is the discipline demand matrix at iteration t. The derivative $\eta=\partial L_{RAG}/\partial t$ represents the knowledge update rate, calculated as the loss reduction between two adjacent iterations. Here, L_{RAG} denotes the loss function of the RAG module, which evaluates the semantic similarity and engineering consistency between retrieved knowledge and current design requirements.

In the Subtask Execution Area (Area c), when multiple agents execute subtasks, conflicts may arise due to conflicting local optimization objectives (e.g., simultaneously pursuing lightweight design and increased strength), leading to non-cooperative game dilemmas. To coordinate agent strategies, the Nash Equilibrium is introduced to describe optimal strategy selection under conflicts. The optimization strategy for the i-th agent A_i satisfies:

$$\begin{aligned} &\max_{x_i}\left[U_i(x_i,x_{-i}) - \rho\cdot\| x_i - x_i^{\mathrm{LLM}}\|_2\right] \\ &\text{s.t.}\quad g_j(x_i)\le 0 \quad (j=1,2,\ldots) \end{aligned} \tag{4}$$

In this equation, the objective function U_i balances the agent's performance and interdisciplinary collaboration, defined as a trade-off between discipline contributions and conflict penalties:

$$U_i = \boldsymbol{W}_G \cdot x_i - \alpha \cdot \sum_{k \neq i} \left\| \boldsymbol{W}_G(k,:) \cdot x_i \right\|_2^2 \tag{5}$$

Here, $\boldsymbol{W}_G(k,:)$ denotes the k-th row of the multidisciplinary coupling matrix, corresponding to the contribution weight distribution of the k-th discipline across the design variables and constraints, and $\boldsymbol{W}_G \cdot X_i$ reflects the interdisciplinary performance contribution of the design solution X_i, i.e., how the chosen design variables simultaneously influence multiple disciplinary objectives. The α is the conflict penalty coefficient (suppressing interdisciplinary conflicts, e.g., in scenarios where high-strength materials are difficult to process). The variables and factors x_i represent the design variables (e.g., geometric dimensions) of agent A_i, x_i^{LLM} is the semantic-guided solution generated by LLMs, and ρ is the semantic-numerical synergy strength factor, defined as a weighting coefficient that balances the relative influence of semantic guidance (x_i^{LLM}) and numerical optimization (x_i) in the agent's objective function. The explicit constraint $g_j(x_i)$ is defined as follows: for the stress constraint of the mechanical agent A_1, $g_1(x_1)=\sigma(x_1)-[\sigma]\leq 0$, indicating that the design stress $\sigma(x_1)$ must be less than the allowable stress $[\sigma]$ to satisfy the stress design requirements.

2.2 Multi-Role Agent Hierarchical Reasoning Mechanism

Given the multi-stage and role-differentiated nature of complex engineering design tasks, this study introduces a hierarchical multi-agent reasoning mechanism that enables structured decision-making and iterative optimization. Built upon the ReAct framework [17], the proposed system integrates four specialized agents—Requirements Analyst, Task Planner, Designer, and Results Feedback Agent—into a collaborative architecture governed by the SNS-Loop. Each agent operates under the LLM-driven semantic reasoning paradigm while forming closed numerical verification loops with ROSMs, thereby overcoming the limitations of traditional single-agent design methods.

Requirements Analyst: This agent is responsible for translating user intentions into executable design objectives and constraints. It adopts a dual-channel semantic extraction mechanism, simultaneously parsing explicit requirements (e.g., load conditions) and implicit constraints (e.g., manufacturability). To enable accurate knowledge support, the agent relies on a domain-specific RAG knowledge base. This knowledge base was constructed from three sources: (1) historical mechanical design cases from our internal repository, (2) engineering standards and handbooks (e.g., stress limits, material property tables), and (3) relevant peer-reviewed publications and technical reports. All documents were segmented into passages of approximately 300–500 tokens, with metadata such as material type, structural feature, and design objective manually tagged

to enhance retrieval precision. The embeddings were stored in a FAISS-based vector database. Leveraging this system, the Requirements Analyst can dynamically retrieve design precedents and domain constraints in real time, thereby assessing feasibility and refining requirement definitions with high accuracy. The retrieval process adopts a vector-based similarity search strategy, with a similarity coefficient threshold set at 0.8. For each query, the top 5 most relevant passages are returned from the knowledge base, with a maximum citation length of 10,000 characters to balance completeness and efficiency. This configuration ensures that the agent receives sufficient technical context without introducing redundant information, thereby improving both retrieval precision and downstream decision quality.

Task Planner: The Task Planner constructs a structured task list by leveraging the contextual understanding capabilities of LLMs. It identifies key subtasks—such as structural analysis and process optimization—and formulates an optimized execution sequence based on two objectives: minimizing the number of design iterations and reducing inter-disciplinary coupling. Specifically, the Task Planner analyzes parameter dependencies and potential conflicts across disciplines. Highly interdependent subtasks are grouped or ordered to minimize back-and-forth iterations, while tasks with fewer external dependencies are prioritized earlier. This dependency-aware sequencing effectively reduces redundant cross-disciplinary feedback loops and stabilizes downstream inputs. The output is a structured task graph that includes task dependencies, execution order, and intermediate validation checkpoints.

Designer: This module adopts a distributed sub-agent architecture, where each sub-agent specializes in a specific engineering discipline. Two core capabilities are implemented: (1) A sensitivity analysis engine based on variance decomposition (Eq. (6)) to screen key variables with high Sobol indices. Specifically, Eq. (6) computes the Sobol sensitivity index S_i, which measures the relative contribution of an input variable X_i to the variance of the system output Y. The numerator term $E_{x-I}[\mathrm{Var}_{xi}(Y|\ X_{-i})]$ represents the expected conditional variance of Y when X_i is fixed, thereby quantifying the independent influence of X_i on the system response. The denominator term $\mathrm{Var}(Y)$ denotes the total variance of the output. By normalizing this ratio, the Sobol index provides a quantitative criterion for identifying key design variables that dominate system behavior. (2) High-precision numerical evaluation via ROSMs invocation, enabling millisecond-level simulations for tasks such as stress prediction, deformation analysis, and modal frequency estimation. These

features allow the Designer to effectively explore and optimize the design space, reducing computational overhead and enabling rapid response in iterative workflows.

$$S_i = \frac{E_{x_{-i}}[\mathrm{Var}_{x_i}(Y \mid X_{-i})]}{\mathrm{Var}(Y)} \tag{6}$$

Results Feedback Agent: The Feedback Agent serves as the evaluation and iteration control component. It applies multi-dimensional threshold criteria—such as stress safety factors, deformation limits, and resonance avoidance bands—to assess the validity of the current design. If violations or deviations are detected, it triggers iterative refinement. The evaluation function for the k-th iteration is defined as:

$$\mathrm{Score}^{(k)} = \sum_{i\in\Omega} w_i^{(k)} \cdot \frac{y_i^{\mathrm{target}} - y_i^{(k)}}{y_i^{\mathrm{target}}} + \lambda \sum_{j\in C} \max\left(0, g_j\left(X^{(k)}\right)\right) \tag{7}$$

In this equation, $\mathrm{Score}^{(k)}$=[Weighted sum of performance deviations]+ λ[Penalty for constraint violations]. In the performance deviation term, $w_i^{(k)}=w_i^{(k-1)}\cdot\exp(-\beta\cdot|y_i^{(k)}-y_i^{\mathrm{target}}|)$ represents the adaptive weight for performance indicator i, where a larger $w_i^{(k)}$ indicates greater deviation from the target and prioritizes optimization in subsequent iterations. Here, Ω denotes the set of performance indicators, y_i^{target} is the target value for indicator i ,and, $y_i^{(k)}$ is the actual value at the k-th iteration. In the constraint violation penalty term, λ is the penalty coefficient, C is the constraint set, and $g_j(X)=y_j-c_j$ quantifies the violation. Iteration terminates when the score change between adjacent iterations falls below an empirical threshold:

$$\left|\mathrm{Score}^{(k)} - \mathrm{Score}^{(k-1)}\right| < \epsilon \ (\epsilon \text{ usually takes } 0.01) \tag{8}$$

2.3 ROSMs Modeling Method

Acknowledging the limitations of LLMs in numerical prediction, this study innovatively employs a multi-agent architecture based on large and small model collaboration to meet the demand for precise numerical prediction in mechanical design tasks. ROSMs, reduced-order models stored locally on a computer, is defined as:

$$Y^{(k)} = M_{ROM}(X^{(k)}) = [m(X), \sigma(X), f_i(X)]^T \tag{9}$$

Where $m(X)$ is the mass prediction model, $\sigma(X)$ is the Von Mises stress prediction model, and $f_i(X)$ is the prediction model for the first i-th non-zero modal frequencies of the component. The specific modeling approach is illustrated in Fig. 2: First, parametric three-dimensional modeling of the target component is

performed using CAD software, followed by finite element modeling and mechanical analysis through simulation software. The finite element analysis process based on Python scripts is then extracted and imported into the design experiment module of the multidisciplinary optimization software. A large-scale sample dataset is generated by traversing design variables. Subsequently, key design variables are screened through global sensitivity analysis, and low-correlation parameters are eliminated to reduce iteration complexity. Finally, a data-driven LROMs based on neural network training is developed to provide real-time numerical prediction capabilities for the agent.

3 Experiments

To evaluate the effectiveness and engineering applicability of the proposed DesAgent framework, a set of validation experiments was conducted using a spinning frame wall plate as a case study. This section details the full experimental process, including design objectives, multi-agent collaboration, ROSMs construction, and quantitative performance evaluation. The experimental results demonstrate DesAgent's capability to execute high-efficiency, constraint-aware optimization in real-world mechanical design scenarios.

3.1 Experimental Setup

The spinning frame wall plate, shown in Fig. 3, is used as the test object. It constitutes the main load-bearing side panel of the spinning frame, providing lateral support for the machine, serving as the mounting base for rollers, spindles, and drive systems, and ensuring overall rigidity and vibration resistance. This component was selected because it is both structurally critical and relatively massive, making it a representative case for lightweight optimization in which reducing material usage must be balanced with maintaining structural integrity and vibration performance. The optimization process includes static load simulations to evaluate stress and deformation under operational conditions (bottom fixed constraint, 400 N vertical top load, and 125 N lateral loads on both sides), as well as modal analysis to ensure that the natural frequencies remain separated from external excitation bands (see Table 1), thereby achieving vibration isolation and resonance avoidance.

Table 1. External excitation frequencies

External incentives	Speed (rpm)	Frequency (Hz)	Safety Margin Frequency (Hz)
Rail 155 Lifting Spindle	12000~19000	200~316.7	190~332.5

Rail 180 Lifting Spindle	12000~17000	200~283.3	190~297.2
Rail 205 Lifting Spindle	12000~15000	200~250	190~262.5
Main Drive Motor	960~1450	16~24.2	15.2~25.4
Ring Rail Motor	1400	23.3	22.1~24.5

3.2 Multi-Agent Workflow Implementation

The collaborative workflow is built upon a ChatGLM-based [18] multi-agent framework, following a closed-loop execution path: Material Selection → Design Sequencing → Mass Iteration → Stress Validation → Deformation Validation → Modal Validation. Each phase is handled by a specialized agent: The Requirements Analyst extracts user-defined goals, retrieves historical cases via a local RAG-based knowledge base, and determines initial design parameters and materials; The Task Planner performs global coupling analysis, constructs a multidisciplinary task graph, and delegates execution to the Designer; The Designer Agent calls ROSMs for rapid parametric simulations including von Mises stress prediction, deformation estimation, and modal response; The Results Feedback Agent verifies outcomes against predefined thresholds and triggers further iterations if necessary. This workflow enables automated, iterative, and traceable design optimization, consistent with engineering best practices.

3.3 ROSMs Construction

To enable real-time, high-accuracy numerical prediction within the DesAgent framework, this study constructs ROSMs based on feedforward neural networks. A total of 1,000 samples were generated by systematically exploring the 20-dimensional design variable space, using parametric CAD modeling and automated finite element simulation workflows. These simulations provided detailed mechanical response data under various load conditions, including stress, deformation, and modal frequencies.

As shown in Figs. 4–6, the training data was preprocessed by applying global sensitivity analysis, which quantified the impact of each design variable on different response metrics. This analysis enabled dimensionality reduction by selecting only the most influential parameters, ultimately identifying eight key variables—Size1, Size3, Size7, Size8, Size12, Size14, Size15, and Size18—for inclusion in the final surrogate models. Figure 7 provides an engineering drawing of the spinning frame wall plate, where the geometric location of each parameter is clearly marked. In this figure, the dimensions labeled as Size1,

Size2, …, Size20 represent potential design variables subject to optimization, while several fixed numerical values (e.g., 460, 885) are shown to indicate functional constraints that cannot be altered. For instance, the height of 885 mm corresponds to the structural support requirement of the wall plate, which must remain constant during optimization. This visualization establishes the correspondence between dimensional values and structural features, which facilitates interpretation of the optimization results.

The neural network architecture consists of three hidden layers with 128, 64, and 32 neurons respectively, using ReLU activation functions to capture nonlinearity. To improve generalization and prevent overfitting, L2 regularization and dropout layers (with dropout rates of 0.3 and 0.2) were applied. In addition, early stopping (with a patience of 20 epochs) and dynamic neuron masking were used during training to further stabilize learning. The models were trained using the Adam optimizer with a learning rate of 0.001, and cross-validation results showed that the average coefficient of determination (R^2) exceeded 0.94 across all target metrics. Each ROSM achieved inference latency under 50 milliseconds, satisfying the efficiency requirements of real-time multi-agent collaboration. It is worth noting that constructing ROSMs requires a one-time training overhead. In our case study, we generated 1,000 simulation samples, executed in parallel batches of ten on an NVIDIA RTX 3080 GPU, which required approximately 4 hours of simulation time. Data preprocessing and neural network training required an additional 1 hour. The final surrogate models were then saved using the savedmodel function for direct invocation by the LLM. Thus, the total training overhead was about 5 hours. Once trained, however, each ROSM enables millisecond-level predictions, which reduces the iterative design cycle from days or weeks to only minutes. This modest upfront investment is therefore offset by significant efficiency gains in subsequent optimization iterations.

3.4 Operational Results and Evaluation Methods

The design process of the spinning frame wall plate is illustrated in Fig. 8. In this case, DesAgent adopts a closed-loop workflow of "requirement analysis–task planning–simulation verification–result feedback." The user's design requirements are entered through natural language and translated into structured constraints by the Requirements Analyst. Based on multidisciplinary coupling relationships, the Task Planner generates an optimal task sequence. The Designer invokes ROSMs to rapidly predict stress, deformation, and natural frequencies, while also retrieving component libraries for part selection. The Feedback Evaluator conducts multidimensional verification of the output scheme and automatically triggers parameter

optimization if constraints are not satisfied. Detailed design results are provided in Supplementary Material 1. Experimental data show that the multi-agent system executed a total of 31 design iterations, invoked ROSMs 40 times, and queried the knowledge base twice. The entire task was completed in 232.03 seconds, with a total computational cost of 12,044 tokens (approximately equivalent to one US dollar under standard GPT-4 inference rates). Compared with conventional design workflows, which often require several weeks, this approach significantly improves design efficiency and validates the engineering practicality of DesAgent in mechanical design tasks.

To evaluate the effectiveness of DesAgent, four mainstream assessment methods were considered (Table 2): task-specific performance metrics, LLM-based evaluation, benchmark testing, and human expert review. Task-specific metrics remain the primary assessment tool, focusing on the accuracy and feasibility of the design output by comparing simulated stress, deformation, and natural frequencies against predefined engineering thresholds. This directly reflects the real-world physical performance of the generated designs and is particularly suitable for assessing constraint satisfaction and optimization quality. In addition, human expert review provides indispensable domain knowledge and professional judgment, ensuring that the evaluation process remains grounded in established engineering practices. LLM-based evaluation was used only in a supplementary role, providing comparative perspectives across design schemes to complement simulation metrics and expert review [19].Benchmark-based assessments, while useful in general natural language processing contexts, lack the domain specificity required to evaluate multi-agent collaboration or engineering-level numerical reasoning, and thus were not adopted as a core method [20,21].

Table 2. Applicability conclusions of evaluation methodologies

Evaluation Methodology	Applicability Assessment	Rationale
Task-Specific Metrics	Applicable	Provides direct validation of design feasibility by comparing simulated stress, deformation, and modal frequencies against predefined engineering thresholds.
LLM-Based Evaluation	Supplementary	Offers comparative perspectives across design schemes to complement physics-based metrics and expert review.
Empirical Benchmarks	Inapplicable	Designed for general NLP tasks, lacking domain specificity for evaluating multi-agent collaboration or engineering-level numerical reasoning

Human Evaluation	Inapplicable	Contributes domain expertise and professional judgment, ensuring evaluations remain consistent with established engineering practices

In conclusion, this study adopts task-specific metrics and LLM-based evaluation as the primary assessment methods, offering a balanced and efficient approach to validate both the physical correctness and semantic completeness of DesAgent's design outputs.

3.5 Ablation Study

To quantitatively validate the necessity and contributions of key components in the multi-agent system, we conducted ablation experiments under the same experimental object and constraint conditions described in Section 3.1. The complete model is the proposed DesAgent framework, which integrates four specialized agents: Requirement Analyst, Task Planner, Designer, and Feedback Evaluator. The baseline performance of this full configuration has been presented in Section 3.4.

The ablation setup involves systematically removing one component at a time while keeping the others unchanged, thereby constructing four comparative variants, as summarized in Table 3. For instance, Variant 1 removes the Requirement Analyst, relying solely on the base model (ChatGLM-4) to interpret user requirements; Variant 2 removes the Task Planner, forcing a single LLM to complete tasks sequentially without explicit role allocation; Variant 3 removes the Designer, leaving only the base model to address stress, deformation, and modal rationality; and Variant 4 removes the Feedback Evaluator, resulting in single-pass generation without iterative refinement.

Table 3 Ablation study configuration

Variant	Ablated Component
Variant 1	Requirements Analyst
Variant 2	Task Planner
Variant 3	Designer
Variant 4	Results Feedback Agent

The evaluation metrics considered in this study include the relative mass reduction (ΔMass, %) with respect to the initial design, where a larger value indicates better optimization; the feasible rate (Feasible

Rate) defined as the proportion of solutions satisfying all three constraints; the number of iterations required to obtain the first feasible solution (Iter-Feas); the total wall-clock runtime (Time, s), which accounts for both simulation and inference processes; the number of re-planning events triggered by conflicts or failures (Backtracks), where a lower value is preferred; and the total token consumption (Tokens), which is reported for benchmarking the computational cost.

4 Discussion

In this section, we synthesize the main findings of the study, interpret their engineering implications, and highlight the contributions of the proposed DesAgent framework. The discussion is organized into several parts: first, the analysis of the design outcomes; second, comparative evaluations with existing methods; third, ablation studies of system components; and finally, validations of generalizability across different operating conditions. This structure ensures a comprehensive reflection on both the technical effectiveness and the broader applicability of the proposed approach.

4.1 Analysis of Design Outcomes

The primary objective of the DesAgent-driven design process is to achieve lightweight structural optimization of the spinning frame wall plate while ensuring that key mechanical constraints are met. Specifically, the design must satisfy three critical conditions: (1) the von Mises stress should remain below the allowable limit defined by the selected material (HT150), (2) the maximum deformation should be within the process tolerance, and (3) the natural frequencies of the structure must avoid the external excitation frequency ranges, with a ±5% safety margin to prevent resonance. The specific numerical thresholds are instantiated by DesAgent during the design process based on the selected material and geometry. In practice, the external excitation table and ±5 % safety margins are automatically translated into enforceable modal constraints by the Requirements Analyst and Task Planner agents during iteration.

As illustrated in Fig. 9, the iterative optimization process led to a monotonic decrease in component mass, starting from 51.31 kg and converging to 35.16 kg after ten iterations. The evolution of mechanical performance indicators, shown in Fig. 10, confirms that all optimized designs satisfy the stress constraint, with values consistently below 50 MPa. The deformation results remain within acceptable limits for the first six iterations, not exceeding the 0.2 mm threshold set by manufacturing process guidelines. Modal analysis conducted on the feasible solutions from iterations 1–6 indicates that the fifth and sixth iterations effectively

shift the first twelve non-zero natural frequencies outside the external excitation bands, as shown in Fig. 11 and detailed in Table 1. Based on a comprehensive evaluation of weight reduction, structural safety, and resonance avoidance, the sixth iteration was selected as the final design scheme. Compared to the initial baseline, this design achieves a 21.2% reduction in material consumption while maintaining compliant stress levels, minimal deformation, and sufficient vibration isolation. Detailed dimensional adjustments are summarized in Table 4, while improvements in mechanical response metrics are provided in Table 5.

Table 4. Dimensional optimization results

Parameter	Initial/Empirical Value (mm)	Optimized Value (mm)	Change (%)
Size1	440	447.47	+1.7
Size3	80	79.81	-0.2
Size7	300	298.08	-0.6
Size8	100	119.76	+19.76
Size12	145	147.18	+1.5
Size14	360	370.58	+2.9
Size15	30	22	-26.7
Size18	255	239.47	-6.1

Table 5. Results of design optimization for the spinning frame wall plate.

Response	Initial/Empirical Value	Optimized Value	Improvement (%)
Mass	51.31Kg	40.42Kg	-21.2
Max Deformation	0.15mm	0.19mm	+26.7
Max Von Mises Stress	3.45MPa	3.65MPa	+5.8

Finite element validation of the sixth iteration, as shown in Fig. 12, confirms the accuracy of the surrogate model predictions. The deformation and stress contours illustrate that the structure performs within allowable limits under operational loading, thereby validating the reliability of DesAgent's automatic optimization pipeline.

The results of this study further highlight the necessity of adopting a multi-agent collaborative system. While LLMs are not designed for numerical computation, they provide significant advantages in natural language understanding, task analysis, and task planning. Specifically, DesAgent can: (i) interpret user inputs expressed in non-technical language and automatically extract design objectives, constraints, and available

resources; (ii) analyze coupling relationships across tasks such as material selection, structural analysis, and modal analysis; and (iii) schedule and coordinate subtasks to resolve conflicts. These capabilities demonstrate how a multi-agent architecture bridges semantic-level design intent with numerical-level verification, ensuring systematic and efficient design optimization even in problems of relatively low complexity.

4.2 Comparative Evaluation

To further assess the practical performance and generalizability of DesAgent, its design outputs were compared with those generated by several mainstream LLM-driven design paradigms, including GPT-4 reasoning mode, DeepSeek-R1, DeepSeek-V3, ERNIE Bot, and IFlytek Spark, as well as a scheme produced by an experienced human designer. In this study, GPT-4 was employed as a supplementary benchmark. Its assessments were not considered inherently objective but were instead used to complement physics-grounded simulation indicators and expert review. Evaluation criteria included design completeness, engineering computation depth, optimization efficiency, and reasoning transparency, with the results summarized in Table 6. In this table, both the GPT-4 assisted evaluation and the expert panel review adopt a 100-point scale, ensuring a standardized and comparable basis across different design approaches.

Table 6. GPT-4 evaluation results

LLMs	Score	Expert Panel Score (Mean ± SD)	Advantages	Limitations
DesAgent	96	94.3±3.1	Extensive iterative optimization cycles, detailed documentation from preliminary design to multi-stage refinements, precise computations across stress, mass, and modal resonance metrics, demonstrating exceptional engineering analysis and optimization rigor.	Occasional verbosity in explanations, though overall robust and comprehensive.
DeepSeek-R1	92	91.0±4.5	Comprehensive coverage of structural design, dynamic matching, and manufacturing processes; rigorous iterative optimization, stress/modal analyses, and ANSYS simulations, reflecting profound engineering expertise.	Redundant details in some descriptions, yet maintains strong professionalism and innovation.
GPT-4	88	87.2±5.0	Well-structured framework	Insufficient quantitative

Reasoning			encompassing structural design, dimensioning, drive system control, and simulation/validation recommendations.	engineering calculations and iterative optimization data, lacking analytical depth compared to alternatives.
DeepSeek-V3	85	80.6±4.1	Clear articulation of critical dimensions, structural layouts, and drive system control, demonstrating foundational component design competence.	Oversimplified engineering computations and simulations, lacking rigorous iterative refinement and numerical validation.
ERNIE Bot	80	81.4±5.3	Coherent conceptual framework with holistic descriptions of wall plate structures, dimensions, and functional zones, suitable for preliminary design phases.	Absence of detailed engineering computations, simulation validations, and optimization processes, primarily conceptual rather than technical.
iFlytek Spark	86	78.5±4.0	Detailed documentation spanning design specifications, manufacturing processes, assembly protocols, and quality control, showcasing thorough production lifecycle considerations.	Inferior to DeepSeek-R1 and DesAgent in engineering simulations, numerical optimizations, and dynamic analyses.
Human Designer's Scheme	93	92.1±3.7	Demonstrated strong structural integrity and engineering computation depth, with extensive use of professional simulation software to validate stress, deformation, and modal performance; the design shows high practical feasibility and notable innovation	Extremely time-consuming process (≈10 days), significantly slower than DesAgent (232 s) and other LLM-assisted methods (typically 1–2 minutes), resulting in poor efficiency despite high-quality output.

DesAgent achieved the highest overall score of 96, reflecting its ability to perform multi-iteration optimization, incorporate both stress and modal analysis, and produce detailed, data-supported engineering

decisions. In contrast, while DeepSeek-R1 and GPT-4 reasoning mode also performed well, their designs were either lacking in iterative feedback or had limited depth in numerical computation. Methods like ERNIE Bot and IFlytek Spark presented clear conceptual logic but failed to provide simulation-backed validation or rigorous optimization procedures, which are critical in practical mechanical design contexts. The human designer also obtained high scores in both GPT-4 evaluation and expert panel review, comparable to the top-performing methods. However, the design process required approximately ten days, which is considerably longer than DesAgent (232 seconds) and other LLM-assisted methods (typically 1–2 minutes).

These results suggest that DesAgent not only excels in automation and design quality but also outperforms existing LLM-based frameworks in delivering engineering-grade outcomes with explainable reasoning and physical credibility. The combination of hierarchical agent coordination, numerical-surrogate integration, and constraint-driven optimization provides a robust pathway for intelligent, low-cost, and high-performance mechanical system design.

4.3 Analysis of Ablation Results

Table 7 summarizes the averaged results (± standard deviation) across ten repetitions for both the complete DesAgent model and its ablated variants. When the Requirement Analyst was removed (V1), the system relied solely on the base model to interpret user requirements. This weakened the accuracy and efficiency of demand recognition and led to a moderate increase in total runtime. Removing the Task Planner (V2) further resulted in a significant rise in backtracking events (≈ 5.4) and the number of iterations needed to obtain the first feasible solution (Iter@Feas ≈ 9.8), which highlights the crucial role of task decomposition and planning in enhancing efficiency and reducing computational cost.

Table 7. Results of ablation experiments for DesAgent framework

Variant	Mass (%)	Feasible Rate (%)	Iter_Feas	Times (s)	Tokens ($\times 10^3$)
Ours (Full)	21.2±1.4	100.0/±0.0	6.0±1.1	232±19	12.0±0.9
V1	16.1±1.7	80.0±10.2	9.2±3.9	355±33	10.8±0.8
V2	10.5±1.9	50.0±14.1	9.8±2.7	610±75	9.5±0.7
V3	12.8±1.4	70.0±15.3	7.9±2.2	4280±410	8.7±0.6
V4	8.7±1.8	0.0	0.0	28±6	4.1±0.5

A more severe degradation was observed when the Designer was removed (V3). Without the ability to invoke reduced-order surrogate models (ROSMs), the framework was forced to rely exclusively on full-scale finite element analyses. Consequently, the runtime escalated dramatically from 232 s to approximately 4,280 s (an 18.4× increase). Moreover, the absence of rapid "fast-loop" corrections within the SNS-Loop resulted in a substantial reduction in both mass optimization (ΔMass) and feasible rate. This outcome is consistent with the design rationale presented in Section 3.3, where millisecond-level predictions were introduced to support high-frequency corrections and real-time feedback.

Finally, eliminating the Feedback Evaluator (V4) led the system to exhibit a "single-pass failure-prone" behavior. The feasible rate dropped to 0%, indicating that no feasible solution was obtained across repetitions. Because the feedback loop is absent, the pipeline terminates after a single pass, but this single-pass output fails to satisfy the full set of constraints. Taken together, these results clearly demonstrate that each specialized agent—Requirement Analyst, Task Planner, Designer, and Feedback Evaluator—plays an essential role in maintaining system performance, reliability, and efficiency. The removal of any single component causes measurable degradation across feasibility, efficiency, and optimization quality, thereby providing strong empirical evidence for the necessity of the proposed multi-agent collaborative design paradigm. These results also demonstrate that the proposed multi-agent framework effectively governs surrogate-model-based optimization loops, integrating ROSMs within an autonomous workflow to ensure both feasibility and efficiency.

4.4 Generalizability Validation of DesAgent Across Different Parts and Operating Conditions

To evaluate the generalizability of DesAgent, we extended the experimental validation to cover two different structural components: the spinning frame wall plate and the weaving machine frame. For each structure, five operating conditions were considered, resulting in a total of ten independent design scenarios. The five load cases for the wall plate were consistent with those described earlier, with the only difference being the variation in the magnitude of the applied vertical load. Similarly, the five load cases for the weaving machine frame differed in the pressures exerted on its upper surface by components such as the angle wheel and the yarn carrier, which reflects the load-bearing requirements of different weaving machine models. In all cases, the design objective was to achieve weight reduction while ensuring structural soundness, where

soundness was defined in terms of meeting limits on maximum stress, maximum deformation, and resonance avoidance.

The comparative results across all ten scenarios are summarized in Table 8. Performance metrics include mass reduction relative to the initial design, constraint satisfaction, iteration counts, and runtime.

Table 8. Summary of DesAgent performance across multiple components and load cases

Case	Component	Load Condition (N)	Mass Reduction (%)	Constraint Satisfaction	Iterations	Runtimes (s)
1	Wall plate	Original	21.2	(3/3)	6	232
2	Wall plate	350,100	24.3	(3/3)	9	268
3	Wall plate	375,115	22.7	(3/3)	8	257
4	Wall plate	425,135	19.3	(3/3)	4	216
5	Wall plate	450,150	17.8	(2/3)	3	210
6	Weaving frame	800	12.4	(3/3)	3	141
7	Weaving frame	900	10.9	(2/3)	3	139
8	Weaving frame	1000	9.2	(3/3)	2	132
9	Weaving frame	1100	7.9	(3/3)	1	115
10	Weaving frame	1200	6.8	(1/3)	1	107

As shown in Table 8, DesAgent achieved notable mass reduction for both the wall plate (17.8–24.3%) and the weaving frame (6.8–12.4%). In seven out of ten scenarios, all three constraints were satisfied (3/3). In the remaining three cases (two with 2/3 and one with 1/3), partial failures occurred, which may be attributed to extreme loading conditions of the weaving frame. Moreover, the results reveal a clear trend: as the applied load increases, the achievable weight reduction becomes smaller, runtimes shorter, and iteration counts fewer, since additional material and structural integrity are required to withstand heavier loads. This also explains why extreme cases exhibit a lower success rate compared to nominal load conditions. Taken together, these findings indicate that DesAgent demonstrates both robustness under normal operating scenarios and generalizability across different structural designs and load environments.

5 Conclusion

This study presents DesAgent, a novel multi-agent mechanical design framework that leverages the synergy between LLMs and ROSMs to address long-standing challenges in efficiency, cost, and multidisciplinary coordination within complex mechanical design processes. Through the construction of a hierarchical reasoning mechanism and the implementation of a closed-loop SNS-Loop, DesAgent enables an

intelligent workflow from semantic task parsing to numerical validation and iterative optimization. The core contributions of this work are threefold:

(1) It pioneers an LLM-driven, industrial-grade collaborative design paradigm, in which task decomposition, requirement interpretation, and inter-agent coordination are executed through specialized roles;

(2) It introduces a deeply coupled SNS-Loop architecture, where neural network–based ROSMs provide real-time numerical predictions to complement semantic planning, overcoming the traditional limitations of LLMs in engineering computation;

(3) It demonstrates high efficiency and low computational cost, as validated in a spinning frame wall plate case study, where DesAgent achieved a 21.2% reduction in material usage compared to the baseline design (51.31 kg → 40.42 kg) while satisfying all mechanical constraints in just 232 seconds, with a computational cost of only 12,044 tokens.

While DesAgent exhibits strong performance in domain-specific design tasks, several limitations remain. The generalizability of the system is currently bounded by domain-specific training data and the complexity of algorithm integration. To further enhance adaptability and scalability, future work will focus on three key directions:

First, while the current approach relies on parametrized CAD models and task-specific training datasets, which limits its direct applicability to arbitrary design problems, future work will focus on developing automated parametric modeling pipelines and adaptive ROSM construction mechanisms. These improvements will enable surrogate models to be trained directly from user-provided CAD data, allowing DesAgent to dynamically construct lightweight ROSMs on demand and thereby broaden its applicability across different design domains.

Second, we aim to extend DesAgent to support multimodal mechanical design scenarios, incorporating textual, visual, and simulation data to enable richer design intent representation and deeper interaction with physical constraints.

Third, future research will explore multi-component collaborative design, expanding the current agent framework to coordinate the optimization of entire mechanical assemblies, enabling system-level integration beyond single-part optimization.

Fourth, when extending DesAgent to more complex or strongly coupled engineering tasks, new challenges may emerge—such as tighter cross-disciplinary interactions, higher-fidelity surrogate modeling demands, and more intricate multi-agent coordination. Addressing these issues offers promising directions for future development and builds on the strengths demonstrated in this work.

In summary, DesAgent provides a promising pathway for embedding collaborative intelligence into engineering design. It offers a flexible, low-cost, and high-performance solution that is well-positioned to support intelligent design workflows in a wide range of mechanical systems.

504 **Conflict of Interest**

505 No potential conflict of interest was reported by the authors.

506 **Data Availability Statement**

507 The datasets generated and supporting the findings of this article are obtainable from the
508 corresponding author upon reasonable request.

509 **Declaration of Generative AI and AI-assisted technologies in the writing process**

510 During the preparation of this work the author(s) used DeepSeek-R1 in order to [proofread the
511 manuscript by correcting grammatical errors, improving sentence structure, and ensuring consistent verb
512 tenses. No AI was involved in generating or modifying research content, interpreting data, or formulating
513 conclusions]. After using this tool/service, the author(s) reviewed and edited the content as needed and take(s)
514 full responsibility for the originality, accuracy, and integrity of the publication.

515

REFERENCES

[1] Zheng, X. Y., Zhang, X. B., Chen, T. T., and Watanabe, I., 2023, "Deep Learning in Mechanical Metamaterials: From Prediction and Generation to Inverse Design," *Adv. Mater.*, 35(45), p. 2302530. DOI: 10.1002/adma.202302530

[2] Besson, J., Cailletaud, G., Chaboche, J. L.,and Forest, S., 2009, Non-Linear Mechanics of Materials, Springer Science & Business Media, Berlin, Germany. ISBN: 978-90-481-3355-0

[3] Gardner, L., and Mahmud, A., 2006, "Structural Design for Non-Linear Metallic Materials," *Eng. Struct.*, 28(6), pp. 926-934. DOI: 10.1016/j.engstruct. 2005.11.001

[4] Wang, X., Jiang, Z. Xiong, Y., and Liu, A., 2025, "Human-LLM collaboration in generative design for customization," *J. Manuf. Syst.*, 80, pp. 425-435. DOI: 10.1016/j.jmsy.2025.03.012

[5] Tseng, Y.-C., and Chang, Y.-Y., 2025, "Interdisciplinary Co-design with LLM-Based Multi-agents: A Human-AI Platform for Complex Design Challenges," *Proceedings of the 17th International Conference on Human-Computer Interaction (HCII 2025)*, P. L. P. Rau, ed., Lecture Notes in Computer Science, Vol. 15783, Springer, Cham, Switzerland, pp. 396-410. https://doi.org/10.1007/978-3-031-93733-0_25

[6] Zhou, Y., Wang, X., Cao, Q., Qian, L., and Yu, C., 2023, "Relationship between specific work of rupture and blended ratio of two-component blended yarns," *Text. Res. J.*, 93(19-20), pp. 4462-4468. DOI: 10.13475/j.fzxb.20220706901

[7] Shen, Y., Ni, J., Yang, J., and Yu, C., 2022, "Study on the testing of the accelerated point of the floating fiber in the roller drafting process with an improved method," *Text. Res. J.*, 92(1-2), pp. 168-179. DOI: 10.1177/00405175211030881

[8] Shen, Y., Qian, X., and Yu, C., 2022, " A study on the dynamic motion of floating fibers in the double apron drafting process." *Text. Res. J.*, 92(13-14), pp. 2476-2486. DOI: 10.1177/00405175221086046

[9] Ma, B., and Wang, J., 2017, "Study on the fiber distribution in a drafting zone," *J. Text. Inst.*, 108(6), pp. 1057-1064. DOI: 10.1080/00405000.2016.1219448

[10] Sun, N., and Liu, N., 2022, "Study on the accelerated-point distribution of floating fibers in the drafting zone," *Text. Res. J.*, 92(17-18), pp. 3193-3203. DOI: 10.1177/ 00405175211059204

[11] Liu, J., Ji, L., Li, W., Jia, Z., Cheng, J., and Fang, P., 2023, "Efficient optimization design method of centrifugal impellers based on multi-surrogate model," *China Mechanical Engineering*, 34(08), p.899. DOI: 10.3969/j.issn.1004-132X.2023.08.003

[12] Lin, J., Huang, Y., Li, H., Zhou, S., and Huang, Z., 2022, "Design optimization for hydraulic systems of forklift boom based on deep surrogate model," *China Mechanical Engineering*, 33(03), p. 290. DOI: 10.3969/j.issn.1004-132X.2022.03.005

[13] Mo, S., Feng, Z., Tang, W., Dang, H., and Zou, Z., 2020, "Performance optimization of elastic spindle pipe based on neural network and genetic algorithm," *Journal of Textile Research*, 41(04), pp. 161-166. DOI: 10.13475/j.fzxb.20190101306

[14] Han, P., Li, X., Liu, R., Zhang, S., and Yuan, C., 2024, "Prediction method of carding process production quality based on digital twin technology," *Text. Res. J.*, 94(5-6), pp. 713-724. DOI: 10.1177/00405175231217120

[15] Qiu, Y., and Jin, Y., 2023, "Document Understanding-Based Design Support: Application of Language Model for Design Knowledge Extraction," J. Mech. Des., 145(12), p. 121401. DOI: 10.1115/1.4063161

[16] Chen, L., Zuo, H., Cai, Z., Yin, Y., Zhang, Y., Sun, L., Childs, P., and Wang, B., 2024, "Toward Controllable Generative Design: A Conceptual Design Generation Approach Leveraging the Function–Behavior–Structure Ontology and Large Language Models," J. Mech. Des., 146(12), p.121401. DOI: 10.1115/1.4065562

[17] Wang, L., Chen, X., Deng, X., Wen, H., You, M., Liu, W., Li, Q., and Li, J., 2024, "Prompt engineering in consistency and reliability with the evidence-based guideline for LLMs," npj Digital Med., 7(1), p. 41. DOI: 10.1038/s41746-024-01029-4

[18] Zeng, A., Liu, X., Du, Z., Wang, Z., Lai, H., Ding, M., Yang, Z., Xu, Y., Zheng, W., Xia, X., Tam, W.-L., Ma, Z., Xue, Y., Zhai, J., Chen, W., Zhang, P., Dong, Y., and Tang, J., 2022, "GLM-130B: An Open Bilingual Pre-trained Model," arXiv preprint arXiv:2210.02414. https://doi.org/ 10.48550/arXiv.2210.02414

[19] Xiao, Y., Liu, J., Zheng, Y., Xie, X., Hao, J., Li, M., Wang, R., Ni, F., Li, Y., Luo, J., Jiao, S., and Peng, J., 2024, "CellAgent: An LLM-driven Multi-Agent Framework for Automated Single-cell Data Analysis," arXiv preprint arXiv: 2407.09811. https://doi.org/10.48550/arXiv.2407.09811

[20] WANG, X., WAN, G.-W., WONG, S.-Z., ZHANG, L., LIU, T., TIAN, Q., and YE, J., 2024, "ChatCPU: An Agile CPU Design and Verification Platform with LLM," In: Proceedings of the 61st ACM/IEEE Design Automation Conference (DAC '24), Association for Computing Machinery, New York, NY, pp. 1–6. https://doi.org/10. 1145/3649329. 3658493

[21] Abdelnabi, S., Gomaa, A., Sivaprasad, S., Schönherr, L., and Fritz, M., 2024, "LLM-deliberation: Evaluating LLMs with interactive multi-agent negotiation games," CISPA Research Report. https://doi.org/10.60882/cispa.25233028

578
579

Figure Captions List

580

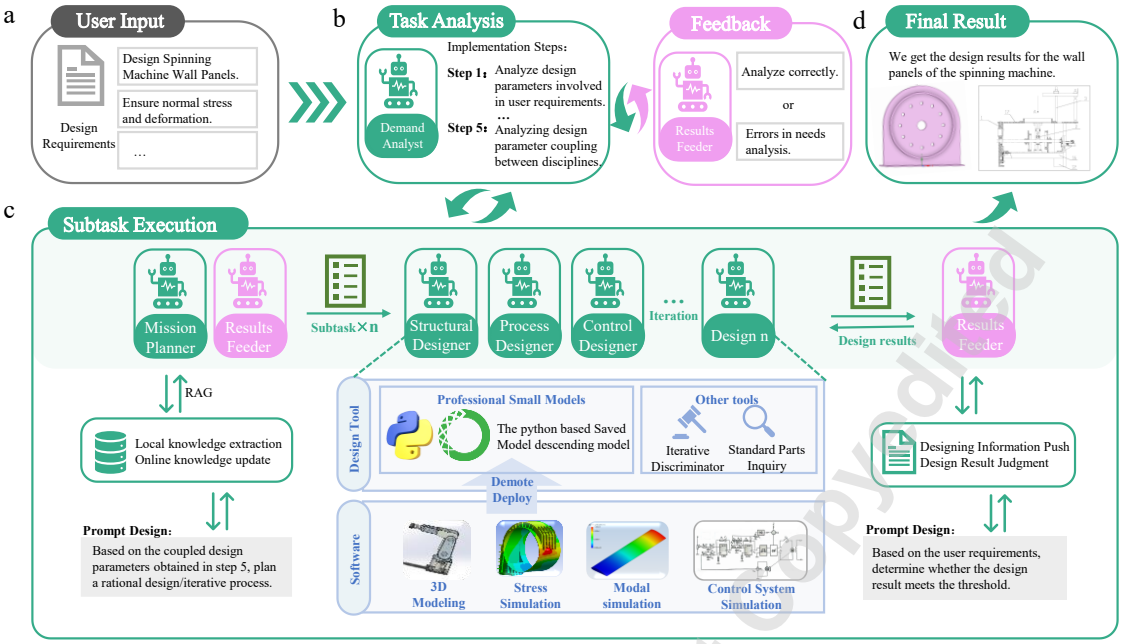

Fig 1. DesAgent architectural framework

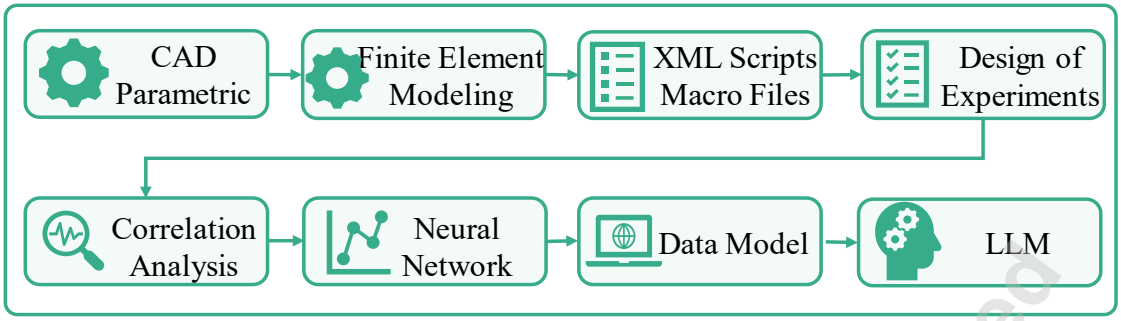

584
585 Fig 2. Fully parameterized ROSMs development workflow
586

Fig 3. Spinning frame wall panel

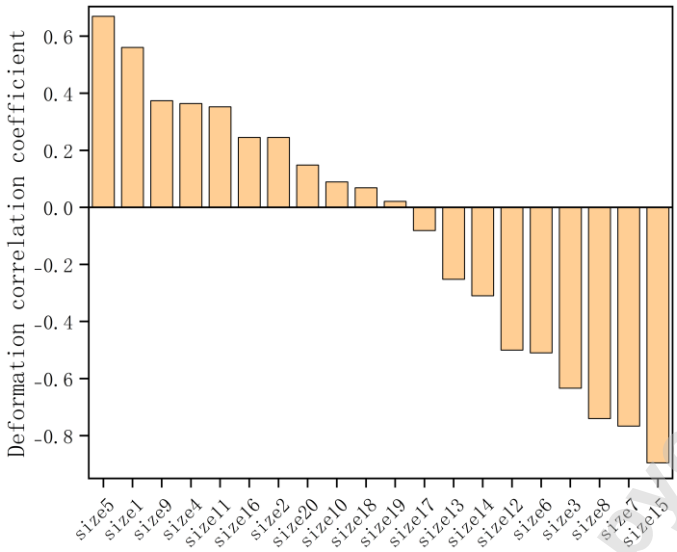

Fig 4. Global sensitivity analysis between deformation and responses

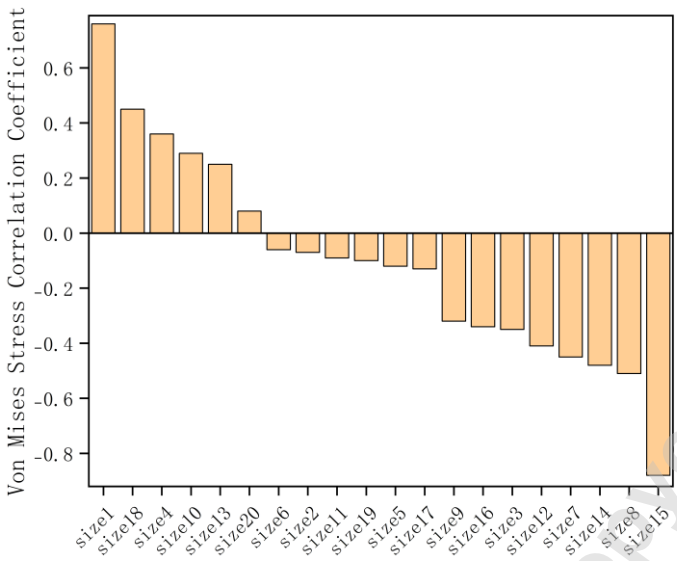

Fig 5. Global sensitivity analysis between von Mises stress and responses

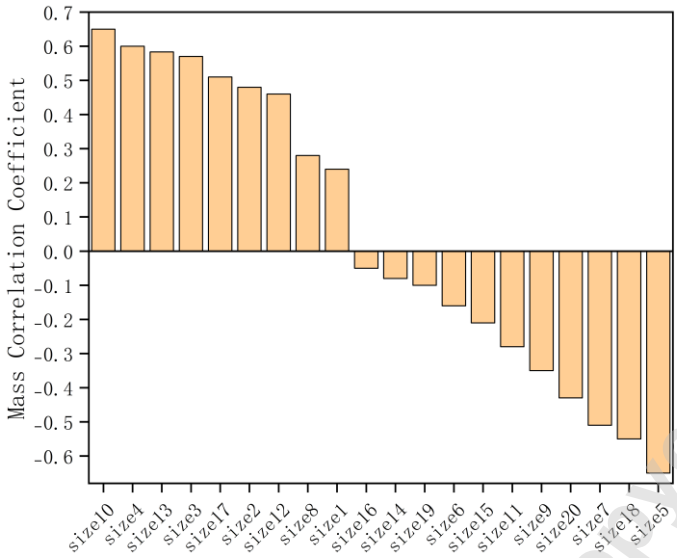

Fig 6. Global sensitivity analysis between mass and responses

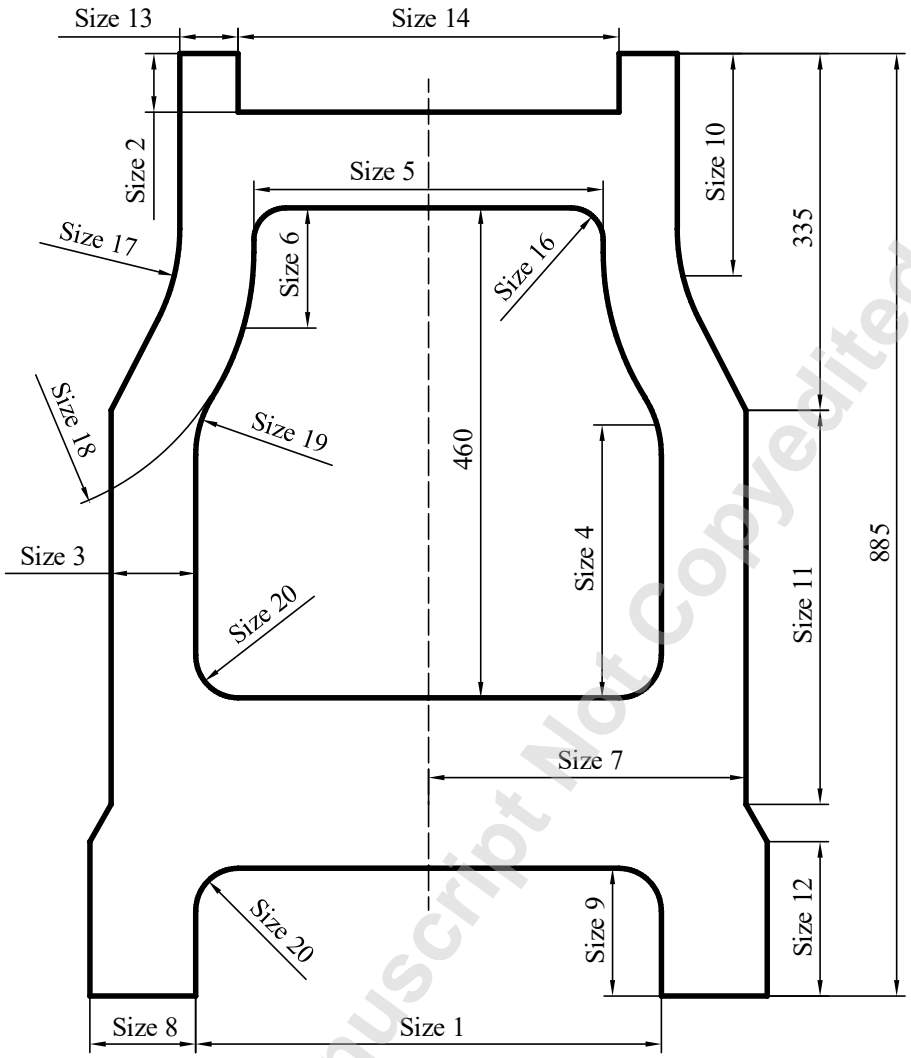

Fig 7. Dimensional layout of the spinning frame wall plate

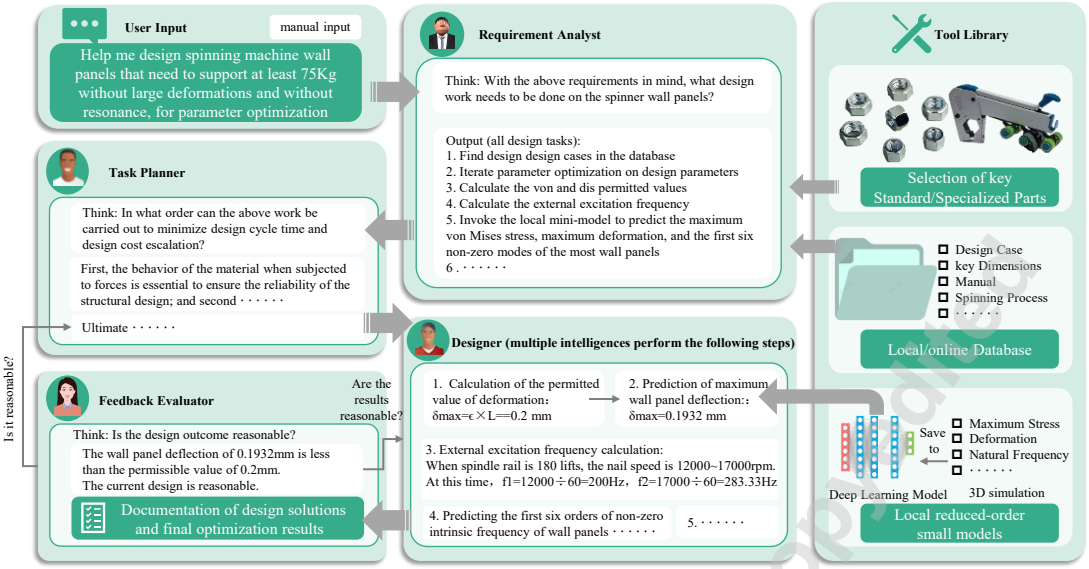

Fig 8. DesAgent operational process

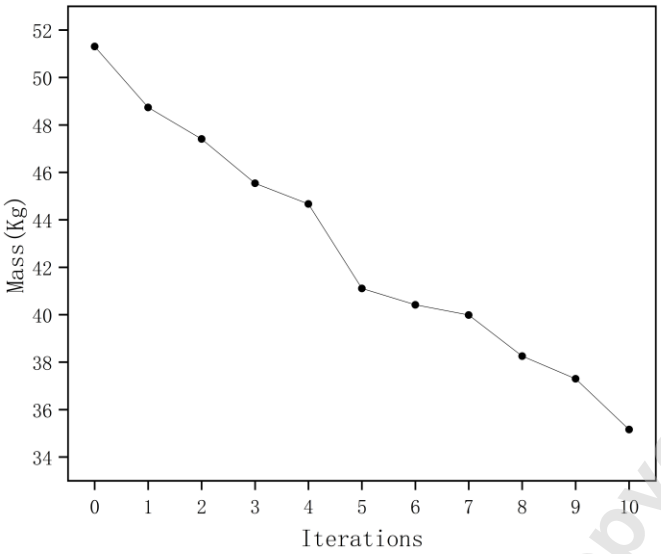

Fig 9. Wall panel mass iteration results

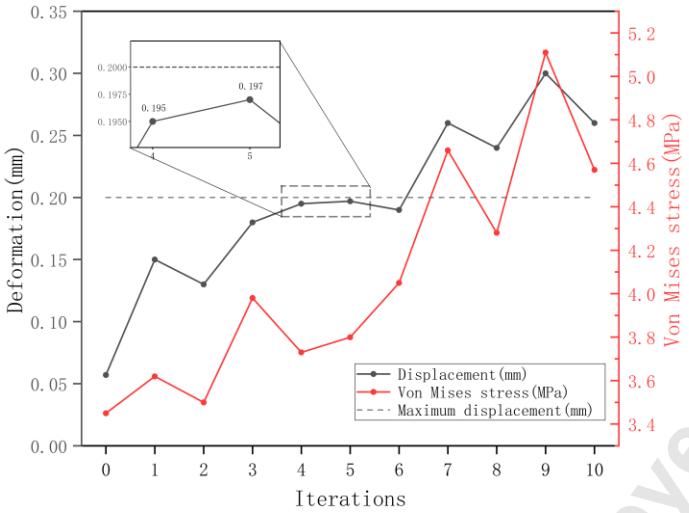

Fig 10. Iterative results of wall panel maximum deformation and von mises stress

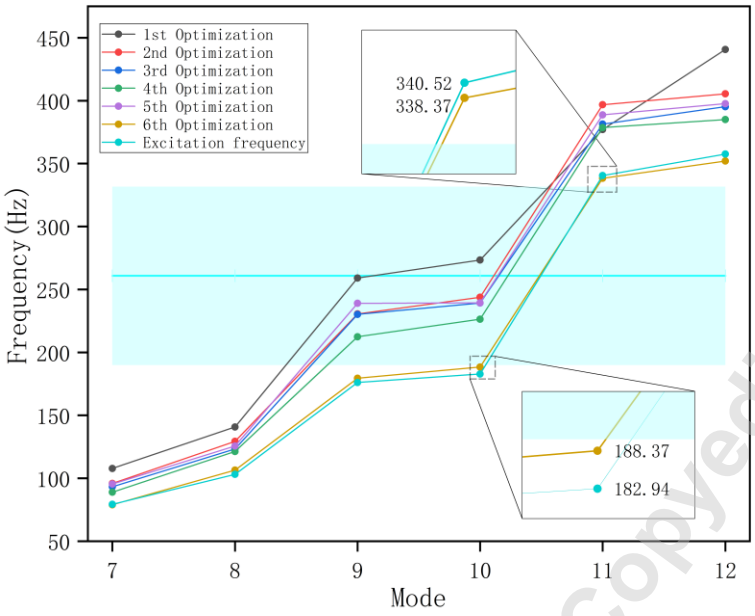

Fig 11. Iterative results of modal natural frequencies at different orders

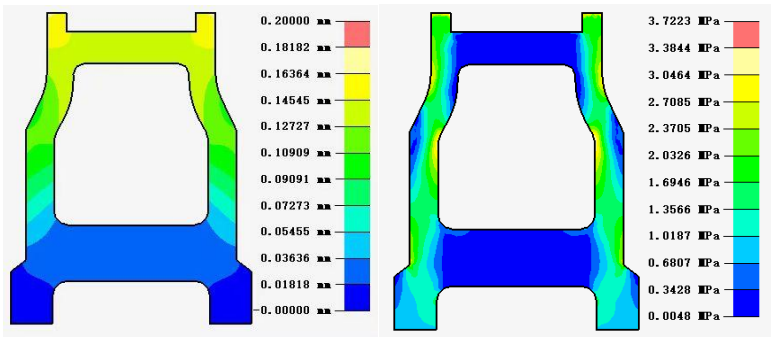

(a) Deformation Simulation (b) Stress Simulation

Fig 12. Simulation results

616 **Supplemental Material**

617 DesAgent operational results:

Design Process Analysis:
In the design project of the spinning frame wall plate, stress analysis should be conducted first. This is because understanding the material's response under stress is crucial for ensuring structural stability and safety. Data such as spindle speed requirements and motor rotational speed affect the dynamic loads borne by the wall plate. Stress analysis helps us understand the impact of these loads on the wall plate structure. Based on this, deformation analysis and modal analysis can be further performed to ensure design precision and optimize structural performance. Therefore, stress analysis is the first step in the design process.
**********(This line is converted into a dividing line in DesAgent)
Material Selection for the Spinning Frame Wall Plate:
Common materials for spinning frame wall plates include steel Q235, Q345, and gray cast iron HT150, HT200, HT250, and HT300. For comparison, Q235, HT150, and HT200 were selected to evaluate the performance of wall plates made from these three materials.
****
Empirical Values for Spinning Frame Wall Plate Dimensions (mm):
80 300 100 440 145 360 30 255
****
Maximum Stress Prediction for HT150 Wall Plate (MPa):
3.45

Mass Prediction for HT150 Wall Plate (Kg):
51.31

****
Maximum Stress Prediction for HT200 Wall Plate (MPa):
3.20

618
619

Mass Prediction for HT200 Wall Plate (Kg):
53.01156234741211

****
Maximum Stress Prediction for Q235 Wall Plate (MPa):
3.23

Mass Prediction for Q235 Wall Plate (Kg):
54.05686569213867

****
Comparison of Stress and Mass for Wall Plates Made from Three Materials:
First, numerical values were rounded to three decimal places:

- HT150 Wall Plate:
- Maximum Stress: 3.450 MPa
- Mass: 51.310 kg

- HT200 Wall Plate:
- Maximum Stress: 3.200 MPa
- Mass: 53.012 kg

- Q235 Wall Plate:
- Maximum Stress: 3.230 MPa
- Mass: 54.057 kg

Next, the mass of the three materials was compared:
- HT150: 51.310 kg
- HT200: 53.012 kg
- Q235: 54.057 kg
From these data, the HT150 wall plate exhibits the lowest mass (51.310 kg). Thus, HT150 is the optimal choice if minimizing mass is prioritized.
****
HT150 was selected as the wall plate material.

****

Rationality Analysis of Maximum Allowable Stress (MPa):
Empirically, the maximum allowable stress for spinning frame wall plates is approximately 50 MPa. For the HT150 wall plate, the predicted maximum stress is 3.450 MPa, significantly below this empirical value. Therefore, the HT150 wall plate meets the allowable stress requirements and ensures sufficient safety. Given its lighter mass, HT150 is an economical and practical choice under safety constraints.

****

First Iteration:
Design parameters: Middle width, hollow section, corner, lower width, height, upper width, thickness, and fillet. Optimized variables: 87.03 mm (eight parameters). Spindle speeds correspond to three levels of rail lifting. Motor speed: 1400 rpm.

****

First Iteration Results — Maximum Stress Prediction (MPa):
3.54

First Iteration Results — Mass Prediction (Kg):
48.73

****

Second Iteration:
Design parameters: Middle width (80 mm), hollow section (300 mm), corner (100 mm), lower width (440 mm), corner height (145 mm), upper width (360 mm), thickness (30 mm), fillet (255°). Spindle speed adjusted with rail lifting. Motor speed: 1400 rpm. Optimized variables: 75.49 mm (eight parameters).
Second Iteration Results — Maximum Stress Prediction (MPa):
3.50

Second Iteration Results — Mass Prediction (Kg):
47.41

****
Third Iteration:
Design parameters: Middle width, hollow section, corner, lower width, corner height, upper width, thickness, and fillet. Considered spindle speed and motor speed requirements.
Third Iteration Results — Maximum Stress Prediction (MPa):
4.08

Third Iteration Results — Mass Prediction (Kg):
45.54

****
Fourth Iteration:
Design parameters: Middle width (80 mm), hollow section (300 mm), corner (100 mm), lower width (440 mm), corner height (145 mm), upper width (360 mm), thickness (30 mm), fillet (255°). Motor speed: 1400 rpm. Optimized variables: 87.03 mm (eight parameters).
****
Fourth Iteration Results — Maximum Stress Prediction (MPa):
3.64

Fourth Iteration Results — Mass Prediction (Kg):
44.68

****
Fifth Iteration:
Design parameters: Middle width (80 mm), hollow section (300 mm), corner (100 mm), lower width (440 mm), corner height (145 mm), upper width (360 mm), thickness (30 mm), fillet (255°). Motor speed: 1400 rpm.
****
Fifth Iteration Results — Maximum Stress Prediction (MPa):
4.33

Fifth Iteration Results — Mass Prediction (Kg):
41.11

****

Sixth Iteration:

Design parameters: Middle width (80 mm), hollow section (300 mm), corner (100 mm), lower width (440 mm), corner height (145 mm), upper width (360 mm), thickness (30 mm), fillet (255°). Motor speed: 1400 rpm.

****

Sixth Iteration Results — Maximum Stress Prediction (MPa):
3.65

Sixth Iteration Results — Mass Prediction (Kg):
40.42

****

Seventh Iteration:

Design parameters: Optimized variables include middle width, hollow section, corner, lower width, height, upper width, thickness, and fillet. Considered spindle speed requirements.

****

Seventh Iteration Results — Maximum Stress Prediction (MPa):
4.51

Seventh Iteration Results — Mass Prediction (Kg):
39.78

****

Eighth Iteration:

Design parameters: Middle width (80 mm), hollow section (300 mm), corner (100 mm), lower width (440 mm), corner height (145 mm), upper width (360 mm), thickness (30 mm), fillet (255°). Optimized variables: 80.61, 280.87, 113.56, 447.7, 140.75, 348.03, 21.33, 235.63 mm.

****

Eighth Iteration Results — Maximum Stress Prediction (MPa):
4.25

Eighth Iteration Results — Mass Prediction (Kg):
38.26

****

Ninth Iteration:
Design parameters: Optimized variables include middle width (80.09 mm), hollow section (274.9 mm), corner width (104.11 mm), lower width (452.54 mm), corner height (138.67 mm), upper width (363.58 mm), thickness (20.38 mm), and fillet (267.06°).
****

Ninth Iteration Results — Maximum Stress Prediction (MPa):
5.06

Ninth Iteration Results — Mass Prediction (Kg):
37.30

****

Tenth Iteration:
Design parameters: Middle width, hollow section, corner, lower width, height, upper width, thickness, and fillet. Optimized variables: 72.95 mm (eight parameters).
****

Tenth Iteration Results — Maximum Stress Prediction (MPa):
4.54

Tenth Iteration Results — Mass Prediction (Kg):
35.15

****

Optimized Minimum Mass (Kg): 35.15
****

Rationality Analysis of Wall Plate Maximum Stress:
The maximum stress predictions across all ten iterations remain within the allowable range (<50 MPa), demonstrating stable and reasonable performance. Minor fluctuations in predicted values suggest high model accuracy.

****

Predicted Deformation of Ten Optimized Spinning Frame Wall Plates (mm):
0.14, 0.13, 0.17, 0.18, 0.20, 0.19, 0.24, 0.24, 0.29, 0.26

Rationality Analysis of Wall Plate Deformation:
The maximum allowable deformation for the wall plate is 0.20 mm. Among the ten optimized results:
- Six deformations (0.14, 0.13, 0.17, 0.18, 0.19, 0.20 mm) meet the requirement.
- Four deformations (0.24, 0.24, 0.29, 0.26 mm) exceed the limit.
****

Modal Resonance Analysis for Spinning Frame Wall Plate:
****

External Excitation Frequency Calculation:
External excitation frequencies are calculated using:
\[f = \frac{n}{60} \]
where \(n \) is rotational speed (rpm). Results:
- Rail 155: 216.67–300 Hz (spindle speed: 13,000–18,000 rpm)
- Rail 180: 216.67–283.33 Hz (spindle speed: 13,000–17,000 rpm)
- Rail 205: 216.67–250 Hz (spindle speed: 13,000–15,000 rpm)
- Motor: 23.33 Hz (speed: 1400 rpm)
****

Predicted First Six Non-Zero Modal Natural Frequencies and Resonance Analysis:
****

1st Iteration Frequencies (Hz)**: 97.35, 131.39, 234.35, 246.46, 399.82, 410.39
- Resonance Risk: Frequencies 234.35 Hz and 246.46 Hz overlap with Rail 155/180 excitation ranges.
****

2nd Iteration Frequencies (Hz): 93.49, 123.91, 230.65, 240.00, 382.45, 396.60
- Resonance Risk: No overlap within ±5% tolerance.

****

3rd Iteration Frequencies (Hz): 90.58, 123.55, 216.35, 230.35, 384.29, 390.91

- Resonance Risk: Frequencies 216.35 Hz and 230.35 Hz overlap with Rail 155/180/205 ranges.

****

4th Iteration Frequencies (Hz)**: 98.27, 128.51, 245.06, 249.17, 397.05, 403.86

- Resonance Risk: Frequency 245.06 Hz overlaps with Rail 205 range (±5%).

****

5th Iteration Frequencies (Hz): 78.94, 106.49, 179.47, 188.37, 338.37, 352.07

- Resonance Risk: Frequencies 78.94 Hz and 106.49 Hz near Rail 205 range (±5%).

****

6th Iteration Frequencies (Hz): 79.40, 103.19, 176.14, 182.94, 324.34, 357.67

- Resonance Risk: Frequencies 176.14 Hz and 182.94 Hz near Rail 180 range (±5%).

****

Optimization Scheme Selection:

The sixth iteration (mass: 40.42 kg) was selected as the final optimized design due to its lowest mass and acceptable stress/deformation performance.

****

Final Design Report:

- Wall Plate Dimensions (mm): 79.808, 298.08, 119.76, 447.46876, 147.17763, 370.57859, 22.397246, 239.473
- Maximum Stress (MPa): 3.65
- Maximum Deformation (mm): 0.19
- First Six Non-Zero Natural Frequencies (Hz): 79.40, 103.19, 176.14, 182.94, 324.34, 357.67
- Optimization Iterations: 10
- AI Agent Analyses: 30
- Local Model Predictions: 40
- Local Knowledge Base Queries: 2

643 Deepseek-R1 operational results:

Design Scheme for the Spinning Frame Side Wall
This scheme is divided into structural design and dynamic matching.
I. Wall Structure Design
(3D coordinate system recommended using SolidWorks or AutoCAD)
Basic Structural Parameters
Section thickness: 30 mm (Dimension 15)
Vertical Layered Design:
1. Lower region (0–145 mm): trapezoidal cross-section
- Bottom width: 440 mm (Dimension 1)
- Top width: 360 mm (Dimension 14)
- Gradient angle: $\theta = \arctan((440-360)/(2\times145)) \approx 15.5°$
2. Middle transition region (145–290 mm):
- Width: 80 mm (Dimension 3)
- Arc transition: 255° (Dimension 18)
- Fillet radius: $R = (300/(2\pi)) \times (255/360) \approx 33.9$ mm
3. Upper functional region (>290 mm):
- Center-to-center hole spacing: 300 mm (Dimension 7)
- Corner width: 100 mm (Dimension 8)

Key Parameter Table

Parameter Code	Value (mm)	Tolerance	Material Treatment
Dimension 1	440	±0.5	Quenched HRC45
Dimension 3	80	±0.2	Chrome plating
Dimension 7	300	±0.1	Precision grinding
Dimension 12	145	±0.3	Stress-relief annealing
Dimension 14	360	±0.5	Shot peening

Dynamic Enhancement Design
- Vibration suppression structure: 6 stiffening ribs on the back (height 15 mm, width 20 mm)
- Natural frequency tuning: mass distribution ensures fundamental frequency > 200 Hz

644

Design Scheme for the Spinning Frame Side Wall
This scheme is divided into structural design and dynamic matching.
I. Wall Structure Design
(3D coordinate system recommended using SolidWorks or AutoCAD)
Basic Structural Parameters
Section thickness: 30 mm (Dimension 15)
Vertical Layered Design:
1. Lower region (0–145 mm): trapezoidal cross-section
- Bottom width: 440 mm (Dimension 1)
- Top width: 360 mm (Dimension 14)
- Gradient angle: $\theta = \arctan((440-360)/(2\times145)) \approx 15.5°$
2. Middle transition region (145–290 mm):
- Width: 80 mm (Dimension 3)
- Arc transition: 255° (Dimension 18)
- Fillet radius: $R = (300/(2\pi)) \times (255/360) \approx 33.9$ mm
3. Upper functional region (>290 mm):
- Center-to-center hole spacing: 300 mm (Dimension 7)
- Corner width: 100 mm (Dimension 8)

Key Parameter Table

Parameter Code	Value (mm)	Tolerance	Material Treatment
Dimension 1	440	±0.5	Quenched HRC45
Dimension 3	80	±0.2	Chrome plating
Dimension 7	300	±0.1	Precision grinding
Dimension 12	145	±0.3	Stress-relief annealing
Dimension 14	360	±0.5	Shot peening

Dynamic Enhancement Design
- Vibration suppression structure: 6 stiffening ribs on the back (height 15 mm, width 20 mm)
- Natural frequency tuning: mass distribution ensures fundamental frequency > 200 Hz

IV. Simulation Verification (ANSYS Workbench)
- Max equivalent stress: <120 MPa (safety factor n = 3.5)
- Fatigue life: >1×10^8 cycles
- Resonance margin: >20%

V. Recommended Implementation Steps
1. Produce 1:5 scale model for modal testing
2. Verify assembly dimensions via 3D printing
3. Conduct bench test with small-batch trial (5 pcs)
4. Optimize stiffener layout
5. Proceed to mass production

Special Note:
When spindle speed > 16,000 rpm, it is recommended to add a copper-based composite damping layer (0.5 mm thick) at the wall mounting surface, which can reduce vibration amplitude by ~40%.

GPT-4 Reasoning operational results:

Spinning Frame Wallboard Design Proposal

Here is a proposed plan for your reference in designing the spinning frame wallboard. The plan is mainly divided into three parts: structural design, dimensional annotation, and drive system control. The details are as follows:

1. Structural Design Description

Material and Processing Technology

It is recommended to use high-strength steel plates (thickness 30 mm, see Dimension 15) as the base material to ensure the rigidity and durability of the wallboard. CNC cutting and machining should be adopted for all parts to guarantee accuracy according to the drawing requirements.

Overall Layout

The wallboard can be divided into the upper, middle, and lower sections, as well as the left and right corners:

- Middle section: width 80 mm (Dimension 3), with a 255° fillet (Dimension 18) for transition. This design is not only aesthetic but also reduces stress concentration effectively.
- Upper section: width 360 mm (Dimension 14), smoothly connected with the middle section.
- Lower section: width 440 mm (Dimension 1), ensuring sufficient support area at the base.
- Hollow design: an internal hollow space with width 300 mm (Dimension 7), reducing overall weight while maintaining necessary strength.
- Corner design: one corner width 100 mm (Dimension 8), another corner height 145 mm (Dimension 12). This ensures tight integration with other parts or walls, achieving seamless assembly.

2. Dimensional Annotations and Details

- Dimension 3 (Middle width 80 mm): Defines the central core area of the wallboard, serving as the benchmark for rigidity and assembly positioning.

- Dimension 7 (Hollow width 300 mm): The hollow design should balance weight reduction and strength. Reinforcement ribs or partial strengthening can be applied to prevent fatigue from excessive hollows.
- Dimensions 8 (Corner width 100 mm) & 12 (Corner height 145 mm): Corners provide structural reinforcement and smooth transition for installation. Ensure proper right angles or rounded transitions during machining to avoid stress concentration.
- Dimensions 1 (Lower width 440 mm) & 14 (Upper width 360 mm): These ensure aesthetics and load-bearing capacity. Pay attention to smooth transitions between upper and lower parts.
- Dimension 15 (Wallboard thickness 30 mm): Determines the main load-bearing thickness. All holes, slots, and transitions must be based on this to ensure assembly accuracy.
- Dimension 18 (Middle fillet 255°): This special curved transition requires high-precision CNC machining to achieve smooth and continuous curves, avoiding burrs and machining errors.

3. Drive System and Speed Requirements

Spindle Speed Control

Depending on different "long rib" sizes (155, 180, 205), the spindle speed range during lifting is as follows:

- Rib 155: 13,000 – 18,000 rpm
- Rib 180: 13,000 – 17,000 rpm
- Rib 205: 13,000 – 15,000 rpm

To meet these requirements, it is recommended to configure a variable frequency drive or servo motor, combined with real-time speed monitoring. Closed-loop control ensures stable spindle speed under different operating modes.

Steel Ring Plate Motor for Automatic Lowering and Reset

The steel ring plate must operate smoothly and reliably. A motor with a fixed speed of 1,400 rpm is recommended, integrated with travel switches and position sensors to achieve automatic lowering and resetting. This ensures smooth motion and precise positioning.

4. Comprehensive Design Suggestions

Modeling and Simulation: Use CAD/CAM software to create a 3D model, ensuring precise dimensions, hole positions, and transitions. Finite element analysis should be performed, especially on hollow and fillet areas.

- Trial and Testing: After initial manufacturing, conduct trial runs focusing on:
  • Assembly accuracy of all dimensions.
  • Stability of spindle operation within specified ranges under different rib lifting conditions.
  • Smoothness and accuracy of steel ring plate lowering and resetting.
- Feedback and Optimization: Based on test data, adjust designs as needed, especially spindle control and structural reinforcements, to ensure long-term stable operation.

Conclusion

This spinning frame wallboard design plan, based on the initial dimensional requirements and modern processing and control technology, ensures structural rigidity and stability. Through careful spindle speed and motor control, stable operation is achieved under different conditions. After completion, further verification through simulation and physical testing is recommended to achieve optimal performance and reliability.

653 Deepseek-V3 operational results:

Spinning Frame Wallboard Design

Spinning Frame Wallboard Design
1. Wallboard Dimensions
According to the provided initial dimensions, the main dimensions of the wallboard are as follows:
- Dimension 3: Middle width = 80 mm
- Dimension 7: Hollow width = 300 mm
- Dimension 8: Corner width = 100 mm
- Dimension 1: Lower width = 440 mm
- Dimension 12: Corner height = 145 mm
- Dimension 14: Upper width = 360 mm
- Dimension 15: Thickness = 30 mm
- Dimension 18: Middle fillet = 255°
2. Spindle Speed Requirements
The spindle speed must remain within the specified ranges under different rib lifting conditions:
- Rib 155 lifting: 13,000 ~ 18,000 rpm
- Rib 180 lifting: 13,000 ~ 17,000 rpm
- Rib 205 lifting: 13,000 ~ 15,000 rpm
3. Motor Speed
The motor used for automatic lowering and resetting of the steel ring plate operates at 1,400 rpm.
4. Design Steps
4.1 Wallboard Structure Design
- Middle section: width 80 mm, thickness 30 mm, with a 255° fillet.
- Hollow section: width 300 mm, ensuring enough space to accommodate spindles and ribs.
- Corners: width 100 mm, height 145 mm, ensuring structural stability.
- Lower section: width 440 mm, providing sufficient support area.
- Upper section: width 360 mm, ensuring stability of the upper structure.
4.2 Spindle Speed Control Design

654

- Rib 155: design the transmission system to ensure spindle speed stays within 13,000 ~ 18,000 rpm.
- Rib 180: adjust the transmission ratio to maintain spindle speed within 13,000 ~ 17,000 rpm.
- Rib 205: further adjust the transmission ratio to keep spindle speed within 13,000 ~ 15,000 rpm.

4.3 Motor Selection and Installation

- Select a motor with a rated speed of 1,400 rpm for the steel ring plate automatic lowering and resetting.
- Ensure stable connection with the transmission system during installation to avoid vibration and noise.

4.4 Material Selection

- Wallboard material should be high-strength, wear-resistant steel or aluminum alloy.
- Ensure good fatigue resistance to withstand long-term high-speed operation.

4.5 Safety and Maintenance

- Consider safety protection measures, such as installing protective covers, to prevent operators from contacting high-speed rotating parts.
- Design for easy maintenance, enabling regular inspections and replacement of vulnerable parts.

5. Summary

Through the above design steps, the structural stability of the spinning frame wallboard and the precision of spindle speed control can be ensured. At the same time, selecting appropriate motors and materials improves durability and safety of the equipment.

657 ERNIE Bot operational results:

Spinning Frame Wallboard Design Overview

Designing a spinning frame wallboard requires comprehensive consideration of structural strength, functionality, manufacturability, and cost-effectiveness. The following is an overview of a wallboard design plan based on the provided initial dimensions and spindle speed requirements. Please note that this is only a conceptual design; detailed calculations and verification should be performed by professional engineers before actual production.

Wallboard Design Overview

1. Overall Structure of the Wallboard

- **Material Selection**: Considering strength and durability, it is recommended to use high-strength steel or alloy steel as the main material of the wallboard.
- **Thickness**: According to Dimension 15, the wallboard thickness is 30 mm.

2. Dimensions and Shape

- **Middle Width**: According to Dimension 3, the middle width of the wallboard is 80 mm.
- **Hollow Width**: According to Dimension 7, the hollow width is 300 mm, used for installation and maintenance of equipment.
- **Corner Width**:
  - Bottom Corner: According to Dimension 8, corner width is 100 mm.
  - Top Corner: According to Dimension 12, corner height is 145 mm (assumed as height, though in practice may indicate special structural requirements requiring clarification). For simplification, this can be considered as an additional width or height feature.
- **Lower Width**: According to Dimension 1, the lower width is 440 mm.
- **Upper Width**: According to Dimension 14, the upper width is 360 mm.
- **Middle Fillet**: According to Dimension 18, the middle fillet is 255° (very close to a full circle; may need confirmation if it should be 270° or a complete circle).

658

3. Functional Areas
- **Spindle Installation Area**: The middle and hollow sections of the wallboard should include spindle mounts and support structures to ensure stability and precision during high-speed rotation.
- **Rib Lifting Area**: The wallboard should include rib lifting tracks and supports to allow smooth lifting at different heights (155 mm, 180 mm, 205 mm).
- **Motor Installation Area**: Reserve an installation space for the motor used for automatic lowering and resetting of the steel ring plate, ensuring stable operation at 1,400 rpm.
4. Spindle Speed Control
- **Spindle Speed**: Based on the requirements, design a transmission and control system to ensure spindle speed can be adjusted within the range of 13,000–18,000 rpm (or lower) under different rib heights.
- **Control System**: Advanced control systems such as PLC or DCS should be adopted to achieve precise control and adjustment of spindle speed.
5. Detailed Design
- **Fillet Treatment**: The fillet treatment of the middle and edge sections should meet safety standards and manufacturing requirements to avoid stress concentration and sharp edges that could cause injury.
- **Welding and Connections**: All parts of the wallboard should be fixed together using high-quality welding or bolted connections to ensure structural integrity and stability.
- **Surface Treatment**: Apply necessary anti-corrosion treatment and surface coatings to improve corrosion resistance and extend service life.
Notes
- **Detailed Calculations**: Mechanical calculations and simulation analysis should be conducted during design to ensure strength and stability under various operating conditions.
- **Manufacturing and Assembly**: Consider the feasibility of manufacturing and assembly to ensure smooth production and installation of the wallboard onto the spinning frame.

- **Cost-effectiveness**: While meeting functional and performance requirements, efforts should be made to reduce material, manufacturing, and installation costs.

Conclusion

This design plan is only a conceptual overview. During the actual design process, detailed design and optimization should be carried out based on specific requirements and conditions. Collaboration with a professional mechanical design team or engineers is recommended to ensure feasibility and effectiveness of the design plan.

662 iFlytek Spark operational results:

Spinning Frame Wallboard Design Plan

I. Design Overview
This spinning frame wallboard design aims to meet specific dimensional and spindle speed requirements, ensuring stable operation and efficient production of the spinning frame. The design fully considers dimensional accuracy, structural strength, and compatibility with other components of the spinning frame.
II. Overall Structural Design of the Wallboard
(1) Dimensions and Layout
- **Dimension 3 (Middle Section)**: Width 80 mm, mainly for support and positioning, ensuring stability of the wallboard in the spinning frame.
- **Dimension 7 (Hollow Section)**: Width 300 mm, used for installation or passage of components such as drive shafts. Precision and smoothness must be ensured to reduce friction and wear.
- **Dimension 8 (Corner Section)**: Width 100 mm, serves as a transitional connection part, enhancing overall structural strength.
- **Dimension 1 (Lower Section)**: Width 440 mm, forming the base support area with sufficient load capacity to withstand operating forces.
- **Dimension 12 (Corner Height)**: Height 145 mm, working together with other parts to form the overall frame structure, ensuring verticality and stability.
- **Dimension 14 (Upper Section)**: Width 360 mm, located at the top for installation and fixation of spinning-related components.
- **Dimension 15 (Thickness)**: Thickness 30 mm, ensuring sufficient strength and stiffness while considering material efficiency and cost control.
(2) Key Part Design
- **Dimension 18 (Middle Fillet)**: Fillet angle 255°. This design reduces stress concentration, improves fatigue resistance, and extends service life. During machining, radius and surface roughness must be strictly controlled to meet quality standards.

663

III. Material Selection
Considering the wallboard must withstand high pressure and friction while maintaining precision and stability, high-strength cast iron is selected. Cast iron provides excellent wear resistance, damping performance, and machinability, meeting operational requirements.
IV. Manufacturing Process
- **Casting Process**: Sand casting is adopted to ensure overall forming quality and internal uniformity. Dimensional accuracy and surface quality must be strictly controlled to avoid defects such as pores or sand holes.
- **Machining Process**: Post-casting machining includes milling, drilling, and boring to ensure dimensional accuracy and surface finish. Critical parts such as Dimension 7 (hollow) and Dimension 18 (fillet) require high-precision equipment to ensure processing quality.
V. Assembly and Commissioning
- **Assembly**: The processed wallboard is assembled with other spinning frame components, ensuring positional accuracy and fit. During assembly, protect the wallboard surface from scratches or damage.
- **Commissioning**: After assembly, the spinning frame is debugged to check wallboard operation and spindle speed compliance. Adjustments to rib lifting positions and motor speeds ensure optimal performance.
VI. Quality Control and Testing
- **Quality Control**: Strict quality management should be applied throughout raw material procurement, casting, machining, and assembly to ensure compliance with design requirements.
- **Testing Methods**: Use CMMs (coordinate measuring machines), hardness testers, and roughness meters to test dimensional accuracy, hardness, and surface finish. Spindle speed can be monitored in real time using photoelectric tachometers.
VII. Maintenance and Care
- **Regular Inspection**: Check the wallboard regularly for wear, cracks, or loosened connections, and address issues promptly.

- **Cleaning and Lubrication**: Keep the wallboard clean by removing dust and debris. Apply lubrication to sliding and transmission parts to reduce friction and wear.

This design plan can be adjusted and refined according to actual requirements. Please let me know if further modifications are needed.